Faraday Discussions

Reaction interferometry with ultracold molecules

Journal:	*Faraday Discussions*
Manuscript ID	FD-ART-12-2023-000175.R1
Article Type:	Paper
Date Submitted by the Author:	09-Feb-2024
Complete List of Authors:	Luke, Jeshurun; Harvard University, Department of Chemistry and Chemical Biology Zhu, Lingbang; Harvard University, Chemistry and Chemical Biology Liu, Yi-Xiang; Harvard University, Chemistry and Chemical Biology Ni, Kang-Kuen; Harvard University, Chemistry and Chemical Biology

CREATED USING THE RSC LaTeX PCCP ARTICLE TEMPLATE – SEE www.rsc.org/electronicfiles FOR DETAILS
PAPER www. rsc.org/faraday_d | Faraday Discussions

Reaction interferometry with ultracold molecules

Jeshurun Luke,[a,b,c†] **Lingbang Zhu,**[a,b,c] **Yi-Xiang Liu,**[a,b,c] **and Kang-Kuen Ni**[a,b,c‡]

We propose to coherently control the ultracold 2KRb $\rightarrow$ K_2 + Rb_2 reaction product state distribution via quantum interference. By leveraging that the nuclear spin degrees of freedom in the reaction maintain coherence, which was demonstrated in Liu and Zhu *et al., arXiv:2310:07620*, we explore the concept of a "reaction interferometer." Such an interferometer involves splitting one KRb molecular cloud into two, imprinting a well-defined relative phase between them, recombining the clouds for reactions, and measuring the product state distribution. We show that the interference patterns provide a mechanism to coherently control the product states, and specific product channels also serve as an entanglement witness of the atoms in the reactant KRb molecule.

1 Introduction

Controlling reaction at the individual quantum state level in a coherent fashion represents the highest level of control and has been a long-standing goal in chemistry and physics. With the development of state-selective preparation of reactants and detection of products, the use of photo-induced coherent control to alter reaction outcomes has proven successful in multiple systems.[1–6] The concept of coherent control of chemical reactions goes beyond photo-induced reactions,[7,8] posing fundamental questions on the extent to which the coherence in the individual quantum states of the reactants influence reactive processes. However, experimental demonstration of such control over reactive scattering, a broad class of reactions, requires initial quantum state preparation, which is challenging on its own.[9]

Recent advances in ultracold atom and molecule technologies allow control over all molecular degrees of freedom, including the electronic, rovibronic, nuclear spin, and partial wave, a requiste for leveraging coherences in reactive processes.[10–24] Out of these degrees of freedom, nuclear spins are one of the most isolated from environments with demonstrated coherence times on the order of seconds.[25–27] These properties prompted a search for its coherence in the context of reactive scattering. Recent experimental demonstration indeed showed that nuclear spin coherence survives through the bimolecular reaction, 2KRb $\rightarrow$ $K_2 + Rb_2$,[28] making them an ideal platform to explore reactive coherent control.

[a] *Department of Chemistry and Chemical Biology, Harvard University, Cambridge, Massachusetts 02138, USA*
[b] *Department of Physics, Harvard University, Cambridge, Massachusetts 02138, USA*
[c] *Harvard-MIT Center for Ultracold Atoms, Cambridge, Massachusetts 02138, USA*
† jeshurunluke@g.harvard.edu
‡ ni@chemistry.harvard.edu

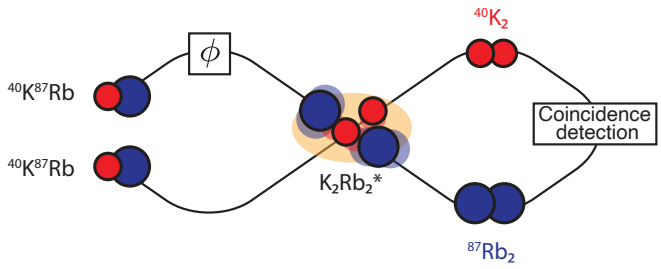

Fig. 1 Conceptual picture of reaction interferometer. Two reactant KRb molecules are initialized in the same coherent superposition state $\frac{1}{\sqrt{2}}(|0\rangle + |1\rangle)$. One molecule picks up a controllable phase ϕ, resulting in $\frac{1}{\sqrt{2}}(|0\rangle + e^{i\phi}|1\rangle)$ before the reaction. The interference patterns could be measured using coincidence detection of the product states. These patterns can be used to quantify the coherence and entanglement in reactants as well as control the product yield in different product channels in a coherent manner.

This survival in coherence suggests that the phase between the nuclear spin states of the reactants carries over to the product nuclear spin wavefunction. Furthermore, because the product molecules are homonuclear, the parity of their rotational states is linked to the parity of the nuclear spins, which has to satisfy the exchange symmetry of nuclei. This connection enables one to regulate the product population in various rotational channels by utilizing the relative phase of the reactant nuclear spin states.

Here, we propose the concept of "reaction interferometry" (Fig. 1), which uses the chemical reaction to recombine two reactant molecules with different phases, in analogy to a beamsplitter in an interferometer for light. In particular, we prepare two clouds of KRb molecules in a superposition of two nuclear spin states $|0\rangle$ and $|1\rangle$ where one cloud is in $\frac{1}{\sqrt{2}}(|0\rangle + |1\rangle)$ and the other is in $\frac{1}{\sqrt{2}}(|0\rangle + e^{i\phi}|1\rangle)$ with a controllable phase difference ϕ imprinted through microwave drives. The outcome of this chemical reaction depends on the relative phase between the two reactants, providing an approach to alter the reaction outcome as well as to probe the short-range dynamics in the reactive scattering process.

In what follows, we will first introduce a theoretical model based on nuclear spin conservation to predict the product wavefunctions dictated through quantum interference. We then present an experimental scheme to prepare relevant reactant states and discuss the expected outcomes of the chemical reaction.

2 Theoretical model

2.1 Coherence in the KRb + KRb → K_2 + Rb_2 reactions

Previous studies characterizing the reaction dynamics probe the rotational product state distribution of K_2 and Rb_2, which, with the exception of a few channels, is in agreement with the statistical model, where the model assumes each quantum state of the product has an equal likelihood to be populated.[29] This indicates

that the underlying dynamics for the ro-vibration degrees of freedom are mostly chaotic.

Coherence, if present, will manifest itself in the degree of freedom most protected from the chaotic dynamics such as within the nuclear spins. Measuring such states directly proves to be difficult so far due to their minuscule energy spacing. Nonetheless, we can probe the parity of the nuclear spin state using the molecule rotational state, given that they need to satisfy homonuclear exchange symmetry constraints. For example, the two potassium (rubidium) nuclei in the K_2 (Rb_2) molecule are indistinguishable Bosons (Fermions). As such, the total wavefunction describing the molecule rotation and spin must be symmetric (antisymmetric) under an exchange of the two nuclei. This requires that a symmetric nuclear spin wavefunction accompanies a symmetric (antisymmetric) rotational state $|e(ven)\rangle$ ($|o(dd)\rangle$). Given the spacing between rotational levels is considerably larger and thus easier to probe, we measure the rotational state of K_2 and Rb_2 to determine the parity of nuclear spin states. With this correspondence, it has been established that nuclear spins are conserved throughout the chemical reaction,[30] a pre-requisite for the search for coherence.

Next, we study the same atom exchange reaction, but this time with rovibronic ground state KRb molecules whose nuclear spins are prepared specifically in an entangled superposition state.[28] This entanglement arises from the spin-spin coupling between the K and Rb nuclei within individual reactant molecules. By measuring the product state distribution, it was found that quantum coherence is preserved throughout the reaction in the nuclear spin degree of freedom. Simultaneously, the product K_2 and Rb_2 molecules inherit the entanglement between the K and Rb nuclei inside the KRb reactants.

2.2 Controlling reactions using interference

Given that coherence survives the chemical reaction, the main objective in what follows is to study the effect of adding a relative phase to one of the reactants. We introduce a formalism to characterize the reactant state and calculate the outcomes. To begin, we first describe the reactant KRb nuclear spin state in the uncoupled basis of the K and Rb nuclear spins $|I^{\mathrm{K}}, I^{\mathrm{Rb}}, m_I^{\mathrm{K}}, m_I^{\mathrm{Rb}}\rangle$. Because $I^{\mathrm{K}} = 4$ and $I^{\mathrm{Rb}} = \frac{3}{2}$ are constants, we do not keep track of them. As nuclear spin states are conserved, and the coherence is preserved, the rearrangement of the nuclei can be understood as a basis transformation,[30] particularly to the basis defined by the tensor product between the coupled K_2 and Rb_2 nuclear spins, $|I^{\mathrm{K_2}}, m_I^{\mathrm{K_2}}\rangle \otimes |I^{\mathrm{Rb_2}}, m_I^{\mathrm{Rb_2}}\rangle$. To show the effect of interference from the relative phase, we present an explicit case with reactants in the following entangled state,

$$\Psi_{\mathrm{KRb}} \otimes \Psi_{\mathrm{KRb}} = \frac{1}{\sqrt{2}}(|-4, \frac{1}{2}\rangle + |-3, -\frac{1}{2}\rangle) \otimes \frac{1}{\sqrt{2}}(|-4, \frac{1}{2}\rangle + e^{i\phi}|-3, -\frac{1}{2}\rangle). \tag{1}$$

After basis transformation from the uncoupled basis to the coupled basis, we obtain the nuclear spin state for the product K_2 and Rb_2,

$$\psi^{\rm nuc}_{\rm K_2,Rb_2} = \frac{1}{2}|8,-8\rangle\otimes(-\sqrt{\frac{2}{5}}|1,1\rangle+\sqrt{\frac{3}{5}}|3,1\rangle) \tag{2}$$

$$+\frac{1}{2}e^{i\phi}(-\frac{1}{\sqrt{2}}|7,-7\rangle+\frac{1}{\sqrt{2}}|8,-7\rangle)\otimes(-\frac{1}{2}|0,0\rangle$$
$$-\frac{1}{2\sqrt{5}}|1,0\rangle+\frac{1}{2}|2,0\rangle+\frac{3}{2\sqrt{5}}|3,0\rangle) \tag{3}$$

$$+\frac{1}{2}(\frac{1}{\sqrt{2}}|7,-7\rangle+\frac{1}{\sqrt{2}}|8,-7\rangle)\otimes(\frac{1}{2}|0,0\rangle$$
$$-\frac{1}{2\sqrt{5}}|1,0\rangle-\frac{1}{2}|2,0\rangle+\frac{3}{2\sqrt{5}}|3,0\rangle) \tag{4}$$

$$+\frac{1}{2}e^{i\phi}(-\sqrt{\frac{7}{15}}|6,-6\rangle+2\sqrt{\frac{2}{15}}|8,-6\rangle)\otimes(-\sqrt{\frac{2}{5}}|1,-1\rangle+\sqrt{\frac{3}{5}}|3,-1\rangle). \tag{5}$$

While coupling two spins $\mathbf{I}_1$ and $\mathbf{I}_2$ together to arrive at $\mathbf{I}$, the coupled spin will be symmetric (S) if $I-I_1-I_2$ is even and antisymmetric (A) if $I-I_1-I_2$ is odd. We group the nuclear spin states based on this symmetry of the coupled K_2 and Rb_2 states and attach the corresponding rotational state of K_2 and Rb_2 with the correct parity (e.g. $|eo\rangle \equiv |N_{K2}=e, N_{Rb2}=o\rangle$ and $|eo\rangle$, $|oe\rangle$, and $|oo\rangle$ are defined similarly) to get the total wavefunction of the nuclei,

$$\psi^{\rm tot}_{\rm K_2,Rb_2} = |SS\rangle|eo\rangle+|AA\rangle|oe\rangle+|SA\rangle|ee\rangle+|AS\rangle|oo\rangle, \tag{6}$$

where

$$|SS\rangle = -\frac{1}{2}\sqrt{\frac{2}{5}}|8,-8\rangle\otimes|1,1\rangle+\frac{1}{2}\sqrt{\frac{3}{5}}|8,-8\rangle\otimes|3,1\rangle$$
$$-\frac{1}{4\sqrt{10}}(1+e^{i\phi})|8,-7\rangle\otimes|1,0\rangle+\frac{3}{4\sqrt{10}}(1+e^{i\phi})|8,-7\rangle\otimes|3,0\rangle$$
$$+\frac{\sqrt{14}}{10\sqrt{3}}e^{i\phi}|6,-6\rangle\otimes|1,-1\rangle-\frac{\sqrt{7}}{10}e^{i\phi}|6,-6\rangle\otimes|3,-1\rangle$$
$$-\frac{2}{5\sqrt{3}}e^{i\phi}|8,-6\rangle\otimes|1,-1\rangle+\frac{\sqrt{2}}{5}e^{i\phi}|8,-6\rangle\otimes|3,-1\rangle, \tag{7}$$

$$|AA\rangle = \frac{1}{4\sqrt{2}}(1+e^{i\phi})|7,-7\rangle\otimes|0,0\rangle-\frac{1}{4\sqrt{2}}(1+e^{i\phi})|7,-7\rangle\otimes|2,0\rangle, \tag{8}$$

$$|SA\rangle = \frac{1}{4\sqrt{2}}(1-e^{i\phi})|8,-7\rangle\otimes|0,0\rangle-\frac{1}{4\sqrt{2}}(1-e^{i\phi})|8,-7\rangle\otimes|2,0\rangle, \tag{9}$$

$$|AS\rangle = -\frac{1}{4\sqrt{10}}(1-e^{i\phi})|7,-7\rangle\otimes|1,0\rangle+\frac{3}{4\sqrt{10}}(1-e^{i\phi})|7,-7\rangle\otimes|3,0\rangle. \tag{10}$$

As illustrated in Eq. 7-10, the population of all parity states depends on ϕ, allowing for an avenue to control reactions coherently. The dependence on ϕ for different rotation parity channels is shown in Fig. 2a. Here, we explore the population distribution of the products with the reactants in the entangled subspace presented

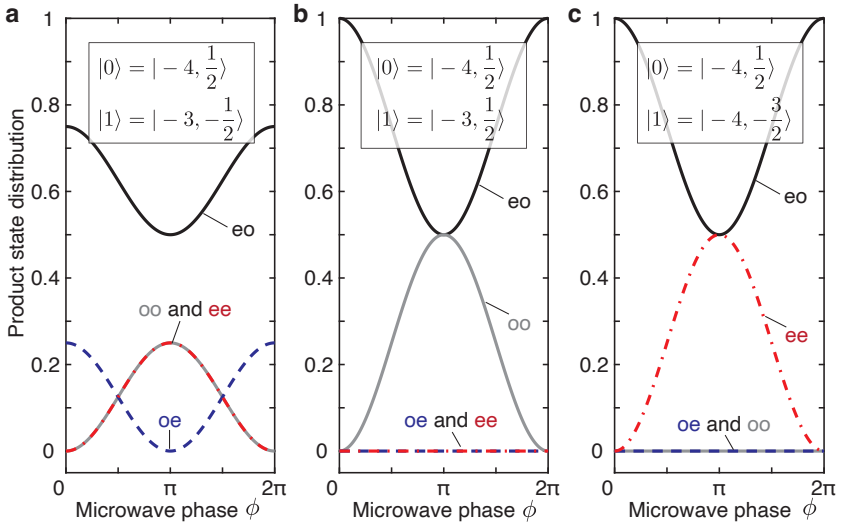

Fig. 2 Product state distributions from reactions between $\frac{1}{\sqrt{2}}(|0\rangle + |1\rangle)$ and $\frac{1}{\sqrt{2}}(|0\rangle + e^{i\phi}|1\rangle)$. Depending on the choice of $|0\rangle$ and $|1\rangle$, one can observe interference arising from (a) K + Rb, (b) K, and (c) Rb nuclear spin subspaces. Black (solid), grey (solid), blue (dashed), and red (dash-dotted) lines represent $|eo\rangle$, $|oo\rangle$, $|oe\rangle$ and $|ee\rangle$ channels respectively. While interference is mathematically demonstrated for (a) following Eq. 1-5, (b) and (c) can be understood with a more intuitive picture. Specifically in (b), with the absence of any relative phase, we expect only the symmetric state to be populated from the exchange symmetry of the two identical potassium atom. With the addition of a relative phase ϕ, the symmetry constraint in the potassium subspace is removed and the anti-symmetric state is populated. Throughout this process, the rubidium channel remains symmetric as there is no change in the Rb subspace with this phase. The control of the interference in (b) by the phase ϕ can be understood similarly to the interference from the relative phase between the two arms of an interferometer. Similar arguments follow for (c), but with the interference in the rubidium subspace instead of the potassium. Within all these reactions, the presence of both $|oe\rangle$ and $|eo\rangle$ populations act as a witness to the entanglement between the K and Rb nuclear spin in the reactant KRb molecule.

in Eq. 1. One can further isolate which subspace interferes by preparing reactants in a product nuclear spin state. For example, for $\frac{1}{\sqrt{2}}(|-4,1/2\rangle + |-3,1/2\rangle) \otimes \frac{1}{\sqrt{2}}(|-4,1/2\rangle + e^{i\phi}|-3,1/2\rangle)$, interference only occurs in the K subspace, and for another state, $\frac{1}{\sqrt{2}}(|-4,1/2\rangle + |-4,-3/2\rangle) \otimes \frac{1}{\sqrt{2}}(|-4,1/2\rangle + e^{i\phi}|-4,-3/2\rangle)$, only the Rb nuclear spins interfere. The choice of states will uniquely alter the population distribution and is calculated similarly as presented for Eq. 1, and the corresponding results are illustrated in Fig. 2.

2.3 Interference patterns reveal the phase coherence and entanglement in reactant KRb molecules

Using the concept of interferometry, we view the chemical reaction as a "beamsplitter" that brings two K atoms and Rb atoms into interference (see Fig. 1). Inspired by literature on entangled photons,[31,32] the interferometer serves to inspect the phase coherence and the entanglement between atoms inside the reactant KRb molecule.

Interference pattern, specifically population oscillation as a function of ϕ, is a signature of coherence. For a completely dephased state, there is no ϕ dependence, and all parity channels are populated. Therefore, destructive interference for a given ϕ in specific channels can be used to identify coherence as was done for our previous work with $\phi = 0$ (Ref.[28]).

Concerning entanglement, reactions between KRb molecules in entangled states result in the coexistence of rotational state pairs with opposite parities, e.g., $|oe\rangle$ and $|eo\rangle$, or $|ee\rangle$ and $|oo\rangle$ (see Fig. 2a), which serves as a witness to the entanglement of the K and Rb atoms in the reactant molecule. On the other hand, when KRb molecules start in a separable product state, as illustrated in Fig. 2b,c, only $|eo\rangle$ and $|oo\rangle$, or $|eo\rangle$ and $|ee\rangle$ coexist.

For example, when the two reactant KRb molecules are identical ($\phi = 0$), entangled KRb states lead to the creation of both $|oe\rangle$ and $|eo\rangle$ products. Reactant KRb molecules in separable product nuclear spin states, on the other hand, only produce $|oe\rangle$. Therefore, in this reaction interferometer, the population correlation of the $|oe\rangle$ and $|eo\rangle$ channels serves as a sufficient and necessary criterion of entanglement in the reactant KRb molecule. This entanglement witness in the reaction interferometer is analogous to using two-photon anti-bunching at a beamsplitter as a signature of entanglement in the well-established literature of entangled photons.[31,32] In Hong-Ou-Mandel experiments,[33] indistinguishable photons bunch. However, as demonstrated in Ref.[31,32], if the input photons are entangled, the corresponding output photons can anti-bunch as the entangled state could have anti-symmetric spatial wavefunctions.

2.4 Entanglement between product K_2 and Rb_2 molecules

Together with the observation of phase coherence maintained throughout the reaction,[28] the product K_2 and Rb_2 will inherit the entanglement from the reactant KRb molecules. It is easiest to see the entanglement between K_2 and Rb_2 when $\phi = 0$ from Eq. 6-10 where only $|SS\rangle|eo\rangle$ and $|AA\rangle|oe\rangle$ terms survive from destructive interference. This entanglement poses questions on whether we can

map out the entangled state with state tomography between K_2 and Rb_2. Ultimately, this depends on the degrees of freedom inspected. Suppose that the product state's hyperfine and rotational degrees of freedom are resolved and that the transitions between states can be driven, then state tomography can be performed to verify the coherence between different product states. However, if only rotational degrees of freedom are resolvable, the nuclear spin information is lost. The products' effective rotational state density matrix is then calculated by performing a partial trace over the nuclear spin degrees of freedom. From such a partial trace, we arrive at a statistical mixture of $|eo\rangle$, $|oe\rangle$, $|oo\rangle$, $|ee\rangle$, as a consequence of entanglement between the nuclear spin state and rotational state given the exchange symmetry constraint of homonuclear molecules. Therefore, no phase coherence between rotational state pairs of different parities will be detectable without nuclear spin resolution. Future experiments could explore rotational resolution in tandem with hyperfine resolution using magnetic field gradients similar to a Stern-Gerlach experiment.

3 Experimental implementation

The calculations in the previous section demonstrate the possibility of coherently controlling the reaction products. Here, we present an experimental scheme to realize such a reaction interferometer. An overview of the experimental sequence is shown in Fig. 3a: A KRb molecular cloud prepared in a single and definite quantum state is first separated into two parts. Then, the two clouds are sequentially addressed and prepared in superposition states with a controllable relative phase. For such addressibility, the individual trap light separating the two clouds are alternatively pulsed to shift the transition resonance (AC stark shift). The molecular cloud in the dark is resonantly addressed using a microwave pulse with a controllable phase while the trapped cloud remain relatively unaffected. After sequentially addressing both clouds, the two clouds are merged and reactions begin. We then readout the quantum state of the reaction product pairs using coincidence detection.

3.1 Adiabatically splitting the reactant cloud into two traps

Coherent control over the relative phase between the two reactant molecules requires selective state control of two molecular clouds. This can be accomplished first by splitting one cloud into two as has been done for atom interferometry with Bose-Einstein condensates[34] and for optical accelerators in studies of collisional processes.[35]

Similarly, we propose a scheme to adiabatically transfer molecules from one broader optical dipole trap (ODT) into two separated tighter ODTs. Initially, molecules are trapped in the cross-section of a horizontal beam (HODT) with a 30 μm beam waist and a vertical beam (VODT) at a 70° angle with a 100 μm waist, which are parameters from an existing experimental setup.[36] Both ODT beams have a wavelength of 1064 nm. Next, we superimpose a copropagating horizontal beam. This beam passes through an acoustic optical modulator (AOM) where the direction and intensity of the beam are electronically controlled via the frequency and the amplitude of a radio frequency (RF) tone, respectively. By driving the

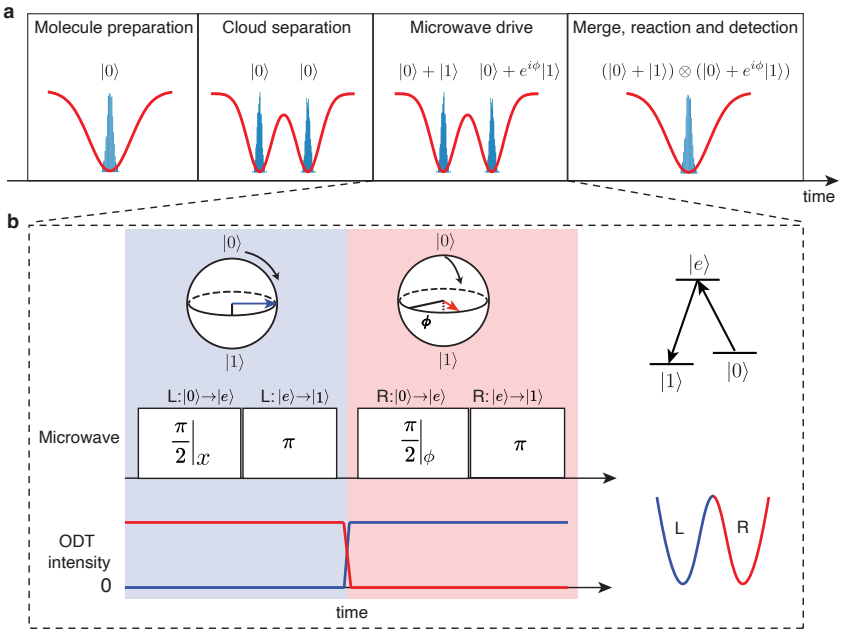

Fig. 3 Experimental timing sequence. (a) After the molecule formation, the traps are adiabatically separated by changing the intensity profile (red curve) of the optical dipole trap. With this separation of the molecular cloud (blue: histogram of the molecules' positions), a microwave sequence can imprint a phase between the two clouds. Finally, we merge the two clouds and measure the product state distribution with coincidence detection. (b) Details of the microwave scheme. By alternating the dark time between the L (blue) and R (red) traps, we introduce local AC Stark shifts, which allows the two clouds to be addressed sequentially. Using an arbitrary waveform generator, we control the phase ϕ between the two $\frac{\pi}{2}$ microwave pulses. Inset shows the three-level system for the sequential microwave transfer.

AOM using two RF tones with carefully selected frequencies, we can generate two traps (L and R) from the copropagating beam, separated by 30 μm and with an equal beam waist of 15 μm. These parameter choices allow us to superimpose a symmetric double well potential with minimal tunneling between them onto the broad trap. Adiabatic transfer of the molecular cloud from the broad trap to the double-well trap is achieved by linearly ramping the L and R trap intensities up while ramping the broad trap down. Minimizing heating during the transfer process is important to maintain a long molecular lifetime. The figure of merit to compare to is the trap height of 12.5 μK and the p-wave barrier height of 24 μK.[10]

To ensure minimal heating throughout the transfer, we perform Monte-Carlo simulations of various trap intensity ramps. To begin, 2000 molecules are drawn randomly from a Maxwell-Boltzmann distribution at a temperature of 0.5 μK inside a potential well formed by the 4 ODT beams with intensities of [10, 0, 0, 10] kW/cm^2 for [HODT, L, R, and VODT] respectively. We scan various ramp times of the ODT intensities to the final value of [0, 7, 7, 10] kW/cm^2, and calculate the effective temperature of the cloud at the end of the ramp by averaging the kinetic energy of all the molecules within a period of 5 ms after the ramp. The 5 ms time period is selected as to capture and average over several trap oscillations. We found a ramp time of 25 ms to give a temperature increase of 0.423 μK, which indicates that the final temperature is below both the aformentioned trap depth and p-wave barrier.

3.2 Imprinting a relative phase between the two KRb molecule clouds

With the two traps separated, we next apply a large AC Stark shift to the relevant transition resonances to address the trap individually. Imprinting a relative phase ϕ can be implemented by rotating the two clouds around different axes on the Bloch sphere, which is realized by alternating the phases of the pulses that couple the two ground hyperfine states, $|0\rangle$ and $|1\rangle$. However, because the transition dipole moment connecting them is negligibly small, we apply a sequential microwave transfer via an intermediate rotational excited state.[37]

At 30 G and 45 V/cm, our typical experimental conditions, we choose the intermediate state $|N, m_N, m_I^{\mathrm{K}}, m_I^{\mathrm{Rb}}\rangle = |1, 0, -4, -\frac{1}{2}\rangle \equiv |e\rangle$ that couples the two hyperfine states in the rotational ground state manifold, $|0, 0, -4, \frac{1}{2}\rangle \equiv |0\rangle$ and $|0, 0, -3, -\frac{1}{2}\rangle \equiv |1\rangle$. N and m_N refer to the rotational angular momentum quantum number and its projection along the quantization axis. To address one cloud selectively, we AC Stark shift the rotation transition of the other cloud away. We alternate the on time for L and R traps to allow a period of dark time to avoid trap inhomogeneity for individual addressing illustrated in Fig. 3b. This approach requires carefully selecting Rabi frequencies to minimize heating from dropping the intensity of a given trap and from off-resonantly driving the other cloud. Specifically, we consider experimentally realizable Rabi frequencies of 1.5 kHz ($|0\rangle \rightarrow |e\rangle$) and 5 kHz ($|e\rangle \rightarrow |1\rangle$). These choices of parameters require a dark time of 270 μs to complete one full $\pi/2_{|0\rangle\rightarrow|e\rangle}$ and $\pi_{|e\rangle\rightarrow|1\rangle}$ pulse set to prepare the superposition, $\frac{1}{\sqrt{2}}(|0\rangle + |1\rangle)$. We quantified the extent of heating during recapture after the free expansion of the cloud using the Monte-Carlo simulation. The extent of heating is quantified by comparing the average kinetic energy throughout 5 ms before and after dropping intensities of the L and VODT

beams. After this window, the average temperature for the molecules in the L trap increases by 0.37 μK, which is still substantially lower than the p-wave barrier. With the completion of the first pulse set to address the molecules in the L trap resonantly, we repeat the same process for molecules in the R trap. During the second pulse set, we use a microwave with a phase ϕ relative to the first pulse set to drive the $\pi/2$ transition. This translates to a different rotation axis on the Bloch's sphere, resulting in a controlled relative phase with respect to the first superposition.

One of the imperfections of the sequence is undesired off-resonant microwave transitions. While the cloud in the dark experiences resonant microwaves of 2228.021 ($|0\rangle \rightarrow |e\rangle$) and 2227.978 MHz ($|e\rangle \rightarrow |1\rangle$), the cloud in a trap of 7 kW/cm^2 has an intermediate state, ($|e'\rangle \equiv |1,-1,-4,\frac{1}{2}\rangle$), that is detuned by 19 kHz from both microwaves. Details on the off-resonant microwaves are illustrated in Fig. 4. To quantify the effect of the off-resonant drive through $|e'\rangle$, we simulate the dynamics for each cloud under the Hamiltonian $H = \Omega_{|0\rangle\rightarrow|e\rangle}|0\rangle\langle e| + \Omega_{|e\rangle\rightarrow|1\rangle}|e\rangle\langle 1| + h.c.$ during the dark time and the Hamiltonian $H = \Omega_{|0\rangle\rightarrow|e'\rangle}|0\rangle\langle e'| + \Omega_{|e'\rangle\rightarrow|1\rangle}|e'\rangle\langle 1| + \Delta|e'\rangle\langle e'| + h.c.$ during the presence of the ODT. Within these equations, Δ corresponds to the detuning, and the Rabi rate $\Omega_{i\rightarrow j}$ describes the coupling between states i and j. Given this coupling is proportional to both the amplitude of the field and the transition dipole moment between the two states, we calculate the Rabi rates of $\Omega_{|0\rangle\rightarrow|e'\rangle}$ and $\Omega_{|e'\rangle\rightarrow|1\rangle}$ by rescaling the transition dipole moments relative to values of $\Omega_{|0\rangle\rightarrow|e\rangle}$ and $\Omega_{|e\rangle\rightarrow|1\rangle}$ defined earlier. Overall, we see fidelities of 0.977 and 0.954 for the state preparation of the R and L clouds, respectively. We discuss the effect of these imperfections of state preparation on the reaction state outcome in Section 3.3. In these calculations, we assume that when the intensity of the R trap is ramped down, the residual $|e'\rangle$ component of the molecules follows one of the eigenstates of the system particularly to the $|e\rangle$ state. In reality, numerous closely spaced avoided crossings during the intensity ramp make it challenging to follow the state perfectly. However, our assumption provides an upper bound on the off-resonant infidelity as maximizing the population in $|e\rangle$ maximizes the population that couples to $|0\rangle$ and $|1\rangle$, leading to the largest phase-dependent error of the final state.

3.3 Merge and reaction

The merge step brings the separated traps with a controlled phase of the reactants back into a single HODT trap within 25 ms. While the clouds recombine, reactions between distinguishable molecules (molecules with a different phase) will preferentially take place because head-on s-wave collisions are 10-100 times faster than p-wave collisions between indistinguishable molecules that have to overcome the centrifugal barrier of 24 μK.[10] Given that the s-wave collision time is on the order of milliseconds, similar to the merge time, ionization detection of products will begin at the start of the merge sequence. State selective ionization is realized using resonance-enhanced multiphoton ionization (REMPI), where we selectively drive the state of interest to an excited state followed by a second excitation to the ionization continuum. The ionized reaction pairs are accelerated using a velocity map imaging setup and detected using a microchannel plate detector (MCP). The ion signals are post-selected to determine products

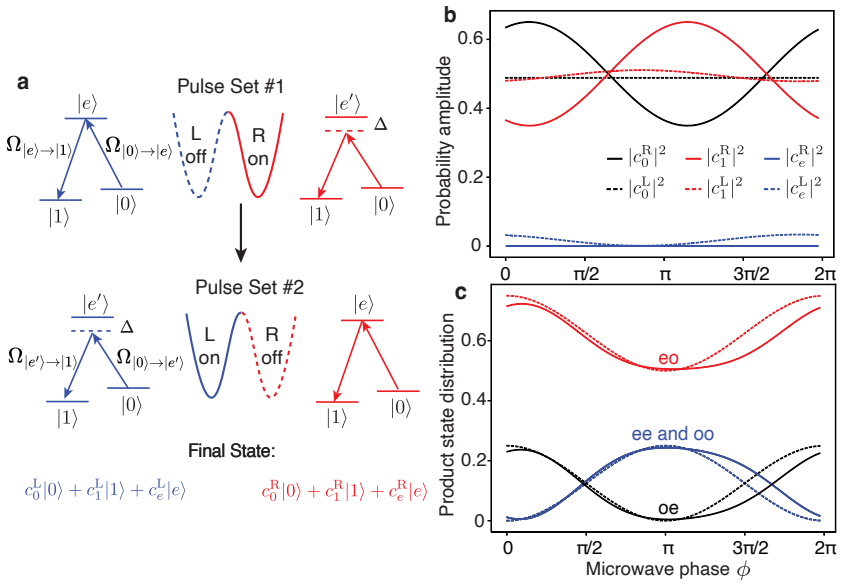

Fig. 4 Infidelities associated with off-resonant driving. (a) Sequential microwave driving scheme. During pulse set #1, the L trap is off, and the microwave pulses are resonant with molecules on the left. However, molecules on the right experience off-resonant driving. Similarly, during pulse set #2, molecules on the left are driven off-resonantly. (b) The state decomposition $|c_i|^2$ for the reactants in the two clouds is shown (dashed refers to the left, and solid refers to the right). These calculations use off-resonant excitation parameters of $\Delta = 19$ kHz, $\Omega_{|0\rangle\to|e'\rangle} = 3$ kHz, $\Omega_{|e'\rangle\to|1\rangle} = 5$ kHz and on-resonant parameters of $\Omega_{|0\rangle\to|e\rangle} = 1.5$ kHz, $\Omega_{|e\rangle\to|1\rangle} = 5$ kHz. (c) Reaction product state distribution with imperfections from off-resonant driving. Dashed lines represent expected population distribution with perfect state preparations. Solid lines are the calculated product state distribution using the state decompositions shown in (b).

from the same reaction event by imposing the momentum conservation criteria, ($\Delta p = |\vec{X}_{K_2} + \vec{X}_{Rb_2}| \approx 0$). The coincidence detection of the products allows us to reconstruct the reaction state distribution; further details on the implementation are discussed in our previous work.[29] For subsequent discussions, we assume the detected population distribution only has contributions from reactions between phase-altered reactants. We then calculate the effect of imperfect state preparation described in Fig. 4 on the observed distribution. The results are shown in Fig. 4c. In these calculations, we neglect the excited state component as its contribution is small (less than 4% of the total population). Overall, by imprinting phases from microwave drive, we can controllably alter the interference of the nuclear spin states, leading to different population outcomes.

4 Conclusions

In summary, we explore the possibility of controlling the reaction using interference by preparing the reactant KRb molecules in superposition states with controllable phases. To achieve phase control, addressing two reactant clouds individually is required and is obtained by splitting an initial cloud into two separate traps. By utilizing trap-dependent AC stark shifts, we individually address each cloud and use microwave pulses to impart selective phase. The performance of this scheme is numerically studied by considering imperfections from undesired off-resonant driving. Observed interference patterns from these reactions provide a platform for coherently controlling reaction products and act as a witness for coherence and entanglement in the reactant molecules. These interference patterns also allow an opportunity to probe the underlying interactions that impart any relative phase in the short range during a chemical reaction.

Acknowledgements

We acknowledge Markus Aspelmeyer for inspiring discussion and sharing the relevant literature of entangled photons. We acknowledge Arfor Houwman for his molecular Hamiltonian code. This work is funded by NSF-EAGER through Grant CHE-2332539 and the U.S. Department of Energy (DOE), Office of Science, Basic Energy Sciences (BES), under Award No. DE-SC0024087, and the Center for Ultracold Atoms (an NSF Physics Frontiers Center).

References

1 D. B. Blasing, J. Pérez-Ríos, Y. Yan, S. Dutta, C.-H. Li, Q. Zhou and Y. P. Chen, *Phys. Rev. Lett.*, 2018, **121**, 073202.
2 L. Zhu, V. Kleiman, X. Li, S. P. Lu, K. Trentelman and R. J. Gordon, *Science*, 1995, **270**, 77–80.
3 A. Shnitman, I. Sofer, I. Golub, A. Yogev, M. Shapiro, Z. Chen and P. Brumer, *Phys. Rev. Lett.*, 1996, **76**, 2886–2889.
4 B. Sheehy, B. Walker and L. F. DiMauro, *Phys. Rev. Lett.*, 1995, **74**, 4799–4802.
5 L. Levin, W. Skomorowski, L. Rybak, R. Kosloff, C. P. Koch and Z. Amitay, *Physical review letters*, 2015, **114**, 233003.
6 R. Levis and H. Rabitz, *The Journal of Physical Chemistry A*, 2002, **106**, 6427–6444.
7 M. Shapiro and P. Brumer, *Principles of the quantum control of molecular processes*, 2003.
8 A. Devolder, P. Brumer and T. V. Tscherbul, *Phys. Rev. Lett.*, 2021, **126**, 153403.

9 W. E. Perreault, N. Mukherjee and R. N. Zare, *Science*, 2017, **358**, 356–359.
10 S. Ospelkaus, K.-K. Ni, D. Wang, M. De Miranda, B. Neyenhuis, G. Quéméner, P. Julienne, J. Bohn, D. Jin and J. Ye, *Science*, 2010, **327**, 853–857.
11 K.-K. Ni, S. Ospelkaus, M. De Miranda, A. Pe'Er, B. Neyenhuis, J. Zirbel, S. Kotochigova, P. Julienne, D. Jin and J. Ye, *Science*, 2008, **322**, 231–235.
12 J. G. Danzl, E. Haller, M. Gustavsson, M. J. Mark, R. Hart, N. Bouloufa, O. Dulieu, H. Ritsch and H.-C. Nägerl, *Science*, 2008, **321**, 1062–1066.
13 F. Lang, K. Winkler, C. Strauss, R. Grimm and J. H. Denschlag, *Phys. Rev. Lett.*, 2008, **101**, 133005.
14 P. K. Molony, P. D. Gregory, Z. Ji, B. Lu, M. P. Köppinger, C. R. Le Sueur, C. L. Blackley, J. M. Hutson and S. L. Cornish, *Phys. Rev. Lett.*, 2014, **113**, 255301.
15 T. Takekoshi, L. Reichsöllner, A. Schindewolf, J. M. Hutson, C. R. Le Sueur, O. Dulieu, F. Ferlaino, R. Grimm and H.-C. Nägerl, *Phys. Rev. Lett.*, 2014, **113**, 205301.
16 J. W. Park, S. A. Will and M. W. Zwierlein, *Phys. Rev. Lett.*, 2015, **114**, 205302.
17 M. Guo, B. Zhu, B. Lu, X. Ye, F. Wang, R. Vexiau, N. Bouloufa-Maafa, G. Quéméner, O. Dulieu and D. Wang, *Phys. Rev. Lett.*, 2016, **116**, 205303.
18 K. K. Voges, P. Gersema, T. Hartmann, T. A. Schulze, A. Zenesini and S. Ospelkaus, *New Journal of Physics*, 2019, **21**, 123034.
19 W. B. Cairncross, J. T. Zhang, L. R. B. Picard, Y. Yu, K. Wang and K.-K. Ni, *Phys. Rev. Lett.*, 2021, **126**, 123402.
20 J. J. Park, H. Son, Y.-K. Lu, T. Karman, M. Gronowski, M. Tomza, A. O. Jamison and W. Ketterle, *Phys. Rev. X*, 2023, **13**, 031018.
21 L. W. Cheuk, L. Anderegg, B. L. Augenbraun, Y. Bao, S. Burchesky, W. Ketterle and J. M. Doyle, *Phys. Rev. Lett.*, 2018, **121**, 083201.
22 M. R. Tarbutt, *Contemporary Physics*, 2018, **59**, 356 – 376.
23 Y. Wu, J. J. Burau, K. Mehling, J. Ye and S. Ding, *Phys. Rev. Lett.*, 2021, **127**, 263201.
24 T. K. Langin, V. Jorapur, Y. Zhu, Q. Wang and D. DeMille, *Phys. Rev. Lett.*, 2021, **127**, 163201.
25 J. W. Park, Z. Z. Yan, H. Loh, S. A. Will and M. W. Zwierlein, *Science*, 2017, **357**, 372–375.
26 P. D. Gregory, J. A. Blackmore, S. L. Bromley, J. M. Hutson and S. L. Cornish, *Nature Physics*, 2021, **17**, 1149–1153.
27 J. Lin, J. He, M. Jin, G. Chen and D. Wang, *Phys. Rev. Lett.*, 2022, **128**, 223201.
28 Y.-X. Liu, L. Zhu, J. Luke, J. Houwman, M. C. Babin, M.-G. Hu and K.-K. Ni, *arXiv preprint arXiv:2310.07620*, 2023.
29 Y. Liu, M.-G. Hu, M. A. Nichols, D. Yang, D. Xie, H. Guo and K.-K. Ni, *Nature*, 2021, **593**, 379–384.
30 M.-G. Hu, Y. Liu, M. A. Nichols, L. Zhu, G. Quéméner, O. Dulieu and K.-K. Ni, *Nature Chemistry*, 2021, **13**, 435–440.
31 A. Fedrizzi, T. Herbst, M. Aspelmeyer, M. Barbieri, T. Jennewein and A. Zeilinger, *New Journal of Physics*, 2009, **11**, 103052.
32 S. Ramelow, L. Ratschbacher, A. Fedrizzi, N. K. Langford and A. Zeilinger, *Phys. Rev. Lett.*, 2009, **103**, 253601.
33 C. K. Hong, Z. Y. Ou and L. Mandel, *Phys. Rev. Lett.*, 1987, **59**, 2044–2046.
34 Y. Shin, M. Saba, T. A. Pasquini, W. Ketterle, D. E. Pritchard and A. E. Leanhardt, *Phys. Rev. Lett.*, 2004, **92**, 050405.
35 A. Rakonjac, A. B. Deb, S. Hoinka, D. Hudson, B. J. Sawyer and N. Kjærgaard, *Opt. Lett.*, 2012, **37**, 1085–1087.
36 L. R. Liu, J. D. Hood, Y. Yu, J. T. Zhang, K. Wang, Y.-W. Lin, T. Rosenband and K.-K. Ni, *Phys. Rev. X*, 2019, **9**, 021039.
37 S. Ospelkaus, K.-K. Ni, G. Quéméner, B. Neyenhuis, D. Wang, M. H. G. de Miranda, J. L. Bohn, J. Ye and D. S. Jin, *Phys. Rev. Lett.*, 2010, **104**, 030402.